

CALCULATION OF ENERGY RELEASE RATES FOR AN AXISSYMMETRIC CRACK
PROBLEM USING THE IMPROVED MODIFIED CRACK CLOSURE INTEGRAL METHOD

H. Grebner* and F.-G. Buchholz**

In combination with the FE-method the improved modified crack closure integral method is used in order to calculate the linear elastic fracture parameters for a crack problem with axial symmetry in form of a penny-shaped crack, extending in a circular cylinder. The cylinder is loaded either by axial tensile forces or by torsional moments, creating Mode I or out of plane Mode III conditions at the circular crack front. As mentioned above the energy release rates G_I and G_{III} and therefrom the corresponding stress intensity factors K_I and K_{III} were calculated as functions of crack/cylinder diameter ratio. In both cases the results are in good agreement with correlating reference values available in the literature.

INTRODUCTION

For the linear elastic fracture analysis by the aid of the finite element method (FE-method) there are available various numerical procedures such as extrapolation methods (Chan et al (1)), superposition methods (Bueckner (2) and Hayes (3)) and numerous kinds of energy methods (4-14). Thereof the improved modified crack closure integral method given by Buchholz (14) has proved to be a very straight forward and highly effective numerical procedure, in combination with higher order finite element discretisations of a cracked structure. The main advantage of this local energy-type method developed from RYBICKI and KANNINEN's modified crack closure integral method (9) is the fact, that for plane mixed-mode crack problems it delivers simultaneously the separated energy release rates $G_i(a)$, $i=I,II$ from just one FE-analysis per crack length a . Furthermore these characteristic fracture parameters or the corresponding stress intensity factors K_i , $i=I,II$ can be calculated from a very limited amount of crack tip data, generated by every standard FE-code.

* Brown, Boveri&Cie AG, Mannheim, FRG;

** Since Jan. 86: Gesellsch.f. Reaktorsicherheit (GRS)mbH, Köln, FRG
Universität-GH-Paderborn, Paderborn, FRG

The following investigation will show, that the method can also be applied successfully to a non-plane crack problem with axial symmetry in form of a penny-shaped crack, located concentrically in a circular cylinder of finite length (Fig.3). The cylinder will be loaded either by axial tensile forces or by torsional moments, respectively (Fig.4), creating crack opening Mode I or out of plane Mode III conditions at the circular crack front perpendicular to the axis of rotation of the cylinder.

CRACK CLOSURE INTEGRAL METHOD

Referring to Fig. 1 and its notations for a pure Mode I condition one can write in accordance with IRWIN (4) the following well known crack closure integral relation

$$\frac{d\Pi}{t da} = G_I(a) = \lim_{\delta a \rightarrow 0} \frac{2}{\delta a} \int_{x=0}^{x=\delta a} \frac{1}{2} \sigma_{yy}(r=x, \phi=0, a) u_y(r=\delta a-x, \phi=\pi, a+\delta a) dx. \quad (1)$$

Equation (1) states, that for an elastic structure the change of the total potential

$$\Pi(a) = W(a) - U(a) \quad (2)$$

due to a crack extension from length a to $a+\delta a$ is equal to the correlated energy release rate $G_I(a)$. Furthermore the change of the total potential is equal to the work which has to be done by the stresses $\sigma_{yy}(, , a)$ at the crack face displacements $u_y(, , a+\delta a)$ (dashed line in Fig.1) in order to close the crack to its original length a again (t thickness of the plane structure). In Eq. (2) $W(a)$ is denoting the work done by the applied external mechanical loads (for example tensional forces or torsional moments (Fig.4)) and $U(a)$ denotes the correlated elastic strain energy of the structure.

According to Buchholz and Meiners (12) Eq.(1) can be transformed into an appropriate FE-representation finally resulting in the following formula

$$G_I(a+\Delta a/2) = \frac{1}{t} \frac{1}{2\Delta a} (F_{y,i}(a)\Delta u_{y,i-2}(a+\Delta a) + F_{y,i+1}(a)\Delta u_{y,i-1}(a+\Delta a)) \quad (3)$$

which is valid in combination with the linear strain element discretisation and finite crack extensions Δa , as shown in Fig.2. From Eq. (3), which will be referred to as crack closure integral method or local energy method-2C, it can be seen that before obtaining one value of the energy release rate $G(a+\Delta a/2)$, two FE-calculations have to be performed with two different crack lengths a and $a+\Delta a$. But different from Eq.(1) the method-2C (Eq.(3)) contains no operation $\lim_{\delta a \rightarrow 0}$, indicating that it is also valid for finite crack extensions $\Delta a \gg 0$. Because crack opening and crack closure are reversible processes for elastic structures this can be concluded in the following way. With the notations given in Fig.2 one can find, that

the nodal point forces $F_{y,i}(a)$, $F_{y,i+1}(a)$ and $F_{y,i+2}(a)$ at the positions $i, i+1$ and $i+2$ have kept the crack of length a closed along the finite increment Δa before crack extension. In consequence of this, these nodal point forces can reverse and cancel the corresponding relative crack face displacements $\Delta u_{y,i-2}(a+\Delta a)$ and $\Delta u_{y,i-1}(a+\Delta a)$ ($\Delta u_{y,i}(a+\Delta a)=0$) of the extended crack with length $a+\Delta a$, which means that they close the crack by Δa to its original length a again. It is emphasized that this property is independent of $\lim_{\Delta a \rightarrow 0}$ and furthermore is holding numerically exact within the actual FE-model under consideration. By the notation $G_I(a+\Delta a/2)$ it is pointed out, that the obtained energy release rate has the meaning of a mean value for a finite crack extension Δa and therefore has to be correlated to $a+\Delta a/2$. Although the method-2C (Eq.(3)) delivers very good results for the energy release rates compared to reference solutions (12) (even with rather coarse FE-discretisation), it has the disadvantage of requiring two FE-calculations for each $G(a)$ -value.

IMPROVED MODIFIED CRACK CLOSURE INTEGRAL METHOD

To avoid the just mentioned disadvantage of the method-2C one can establish in combination with the linear strain element (LSE) discretisation of Fig.2 the following formula

$$G_I(a) = \frac{1}{t} \lim_{\Delta a \rightarrow 0} \frac{1}{2\Delta a} (F_{y,i}(a)\Delta u_{y,i-2}(a) + F_{y,i+1}(a)\Delta u_{y,i-1}(a)), \quad (4)$$

referred to as LSE-formula of 2nd order or as improved modified crack closure integral method-L2 (Buchholz and Meiners (13), Buchholz (14)). From Eq.(4) it is to be seen, that the method-L2 is based on the same correlations between the nodal point forces and crack face displacements of the crack tip area as method-2C (Eq.(3)). But in contrast to Eq.(3), only the crack tip data of just one FE-analysis (for the actual crack length a) is required. This decisive difference, reducing the numerical effort to be made to one half, is based on an assumption made by RYBICKI and KANNINEN (9) for their modified crack closure integral method, given for the fracture analysis of constant strain element (CSE) discretisations of cracked structures. Here, in combination with the numerically more effective LSE-discretisations, the nodal point forces at and in front of the crack tip (positions $i, i+1, i+2$ in Fig.2) are taken correspondingly as approximations for those unknown forces, required to reverse and cancel the crack face displacements at the positions $i, i-1$ and $i-2$, that means to close the crack of length a by a finite increment Δa . Because the just mentioned approximation will only be exact for $\lim_{\Delta a \rightarrow 0}$, no finite formulation can be given for Eq.(4). But it has been shown in (12-15), and the following results will verify this too, that the method-L2 can successfully be applied with finite crack extensions Δa . Furthermore, due to the symmetry of Eq.(4) with respect to the local crack tip position i (Fig.2), the obtained energy re-

FRACTURE CONTROL OF ENGINEERING STRUCTURES – ECF 6

lease rate is correlated to the actual crack length a , although Δa is finite.

If Eqs.(3) and (4) are applied to plane fracture problems, t denotes the thickness of the plane specimen or structure and F/t may be interpreted as nodal point force per unit thickness. In order to extend the method to the actual case of a non-plane problem some additional considerations have to be made.

For load case 1 (axial tensile forces), when the FE-discretisation of the cylinder is based on an axisymmetric TRIAX6-element net, the nodal point forces delivered by the ASKA FE-code are related to one radiant in circumferential direction ($F/t \rightarrow F_i/2\pi r_i$).

For load case 2 (torsional moments), when the FE-discretisation of the cylinder is based on an axisymmetric TICH6-element net, the nodal point forces are related to the circumference ($F/t \rightarrow F_i/2\pi r_i$).

FINITE ELEMENT CALCULATIONS

The method proposed above is applied to a penny-shaped crack located concentrically in a circular cylinder as shown in Fig.3. As mentioned before the cylinder is loaded either by axial tensile forces or by torsional moments, respectively, creating Mode I or out of plane Mode III conditions at the circular crack front.

For the numerical calculations the radius of the cylinder was chosen to 100 mm, while the length of the cylinder was 800 mm. This should be a sufficient length to approximate an infinitely long cylinder for which correlating stress intensity factors are available in the literature. The axisymmetric finite element net used is shown in Fig.4. For symmetry reasons, only the half cylinder has to be modelled. The net-consists of 196 triangular six-node elements. In the case of the axial tensile loading these are standard axisymmetric elements (TRIAX6 in ASKA), while in the case of the torsional loading special "harmonic" elements (TICH6) are used as described by Buck (16). In both cases the net has 445 nodal points. Considering linear elastic material behavior Young's modulus and Poission's ratio were chosen to $E=200,000 \text{ Nmm}^{-2}$ and $\nu=0.3$, respectively.

For the numerical calculations in the case of the axial tensile loading (loading case 1) a constant axial tensile stress $\sigma_0 = 100 \text{ Nmm}^{-2}$ was applied as shown in Fig.4. In the case of the torsional loading (loading case 2) a torsional moment $M_t=2.4987 \cdot 10^4 \text{ Nm}$ is generated by applying the appropriate nodal point forces in the cir-

cumferential direction at the crack free end of the cylinder (Fig.4). Different crack radii a were considered by an appropriate choice of the boundary conditions. In both loading cases crack radius to cylinder radius ratios a/b between 0.1 and 0.9 were studied, with increments of 0.1. For loading case 2 additional finite element calculations were carried out for $a/b=0.05$ and $a/b=0.85$ in order to obtain further energy release rate values at $a/b=0.075$ and $a/b=0.875$ respectively, using method-2C, according to Eq. (3).

ENERGY RELEASE RATES AND STRESS INTENSITY FACTORS

The finite element calculations deliver the crack opening displacements and the nodal point forces in axial and in circumferential directions, respectively, which are necessary to calculate the energy release rate G_I for loading case 1 and G_{III} for loading case 2 by the aid of the presented methods 2C and L2 according to Eqs.(3) and (4), respectively. Using the well known relations

$$K_I = \sqrt{\frac{G_I E'}{1-\nu^2}} \quad (5)$$

(considering plane strain conditions) and

$$K_{III} = \sqrt{\frac{G_{III} E'}{1+\nu}} \quad (6)$$

holding for linear elastic material behavior, the corresponding stress intensity factors K_I and K_{III} can be evaluated from the energy release rates.

A summary of the results is given in Tables 1 and 2, including the additional values for loading case 2 at $a/b=0.075$ and $a/b=0.875$, calculated by means of Eq.(3).

TABLE 1 - Results of the Calculations for Loading Case 1

a/b	G_I/Nmm^{-1}	$K_I/\text{Nmm}^{-3/2}$		$\Delta K_{Irel}/\%$
		Calculated	Reference (17)	
0.1	0.590	362.5	358.5	+1.1
0.2	1.195	512.4	507.6	+0.9
0.3	1.818	632.0	629.0	+0.5
0.4	2.518	743.9	740.4	+0.5
0.5	3.778	861.6	862.4	-0.1
0.6	4.570	1002.2	1001.2	+0.1
0.7	6.479	1193.3	1195.4	-0.2
0.8	10.262	1501.8	1500.3	+0.1
0.9	21.510	2164.3	2228.2	-2.9

Furthermore, in Tables 1 and 2 stress intensity factors are presented, which are available in literature (Tada et al (17)). As mentioned before, these are given for an infinitely long cylinder. According to (17) K_I for loading case 1 may be calculated using the equation

$$\sigma_{net} = \frac{\sigma_o b^2}{(b^2 - a^2)} \quad (7)$$

with

$$K_I = \sigma_{net} \sqrt{\pi a} F_1(a/b) \quad (8)$$

and

$$F_1(a/b) = \frac{2 \sqrt{1-a/b}}{\pi} \left\{ 1 + \frac{1}{2} \frac{a}{b} - \frac{5}{8} \left(\frac{a}{b}\right)^2 + 0.421 \left(\frac{a}{b}\right)^3 \right\} \quad (9)$$

The accuracy of this solution (for an infinitely long cylinder) is reported to be better than 1 percent.

TABLE 2 - Results of the Calculations for Loading Case 2
 (*: Evaluated by Method-2C, Eq.(3))

a/b	G_{III}/Nmm^{-1}	$K_{III}/Nmm^{-2/3}$		$\Delta K_{IIIrel}/\%$
		Calculated	Ref. (17)	
0.075*	$4.004 \cdot 10^{-5}$	2.48	2.26	+0.8
0.1	$7.970 \cdot 10^{-5}$	3.50	3.76	-6.9
0.2	$7.097 \cdot 10^{-4}$	10.45	10.66	-2.0
0.3	$2.453 \cdot 10^{-3}$	19.43	19.62	-1.0
0.4	$5.893 \cdot 10^{-3}$	30.11	30.36	-0.8
0.5	$1.170 \cdot 10^{-2}$	42.43	42.53	-0.2
0.6	$2.090 \cdot 10^{-2}$	56.70	57.31	-1.1
0.7	$3.556 \cdot 10^{-2}$	73.97	74.04	-0.1
0.8	$6.186 \cdot 10^{-2}$	97.56	97.70	-0.1
0.875*	$1.051 \cdot 10^{-1}$	127.16	126.54	+0.5
0.9	$1.298 \cdot 10^{-1}$	141.31	140.00	+0.9

In the case of torsional loading K_{III} may be calculated according to (17) by

$$K_{III} = \tau_N \sqrt{\pi a} F_1(a/b) \quad (10)$$

where τ_N is given by

$$\tau_N = \frac{2 M_t a}{\pi(b^4 - a^4)} \quad (11)$$

and $F_1(a/b)$ can be approximated by

$$F_1(a/b) = \frac{4\sqrt{1-a/b}}{3\pi} \left\{ 1 + \frac{1}{2} \frac{a}{b} + \frac{3}{8} \left(\frac{a}{b}\right)^2 + \frac{5}{16} \left(\frac{a}{b}\right)^3 - \frac{93}{128} \left(\frac{a}{b}\right)^4 + 0.038 \left(\frac{a}{b}\right)^5 \right\} \quad (12)$$

According to (17) the accuracy of this solution is also reported to be better than 1 percent.

Finally, in Tables 1 and 2 the relative differences ΔK_{Irel} and ΔK_{IIIrel} are presented, defined by

$$\Delta K_{Irel} = \frac{K_{Ical} - K_{Ilit}}{K_{Ilit}} \quad (13)$$

and

$$\Delta K_{IIIrel} = \frac{K_{IIIcal} - K_{IIIlit}}{K_{IIIlit}} \quad (14)$$

A graphical presentation of the results is given in Figs. 5 to 8, where energy release rates and stress intensity factors are shown as functions of the a/b-ratio.

DISCUSSION OF THE RESULTS

As can be seen from Table 1, the results gained by the improved modified crack closure integral method (method-L2, Eq.(4)) for loading case 1 are in very good agreement with the values from literature. For a/b-ratios in the region $0.2 \leq a/b \leq 0.8$ the relative deviations ΔK_{Irel} are less than 1 percent. Only for a/b=0.1 and a/b=0.9 ΔK_{Irel} values of more than 1 percent are obtained, namely 1.1 and 2.9 percent, respectively. This is certainly due to the fact, that for finite crack extensions Δa the evaluation of energy release rates by means of Eq.(4) only is an approximation, which probably is not so accurate in the case of a small crack radius (where Δa is half the actual crack radius a) and in the case of a small uncracked ligament. As will be described later, a better approximation is gained in these cases by the use of the more laborious crack closure integral method (method-2C, Eq.(3)). Taking into account that the finite element results, calculated for the cylinder of finite length, are compared to solutions for infinitely long cylinders, the statement at the beginning of the chapter certainly is valid for all a/b-ratios considered. A similar result can be obtained from Table 2 (loading case 2) where ΔK_{IIIrel} is smaller than 2 percent for all ratios a/b, apart from a/b=0.1, for which

ΔK_{IIIrel} rises to 6.9 percent if calculated from Eq.(4). But by using Eq.(3), especially for very small and large crack radii, the accuracy of the results may remarkably be improved for these cases too, as the ΔK_{IIIrel} value of 0.8 percent for $a/b=0.075$ indicates. But it has already been mentioned that the application of Eq.(3) requires two finite element calculations with different crack lengths a and $a+\Delta a$ per $G(a)$ -value, instead of only one in the case of Eq.(4).

To summarize it may be stated, that the extension of the improved modified crack closure integral method to axisymmetric problems delivers an effective numerical procedure for the evaluation of linear elastic fracture mechanical parameters in this field of application too.

REFERENCES

- (1) Chan, S.K., Tuba, I.S., Wilson, W.K.: On the finite element method in linear fracture mechanics. Engng. Fracture Mech. 2 (1970), 1-17
- (2) Bueckner, H.F.: The Propagation of Cracks and the Energy of Elastic Deformation. Trans. ASME 80 (1958), 1225
- (3) Hayes, D.J.: A Practical Application of Bueckner's Formulation for Determining Stress Intensity Factors for Cracked Bodies. Int. J. Fract. Mech. 8 (1972), 157
- (4) Irwin, G.R.: Handbuch der Physik 6 (1958), 551-566
- (5) Rice, J.R.: A path independent integral and the approximate analysis of strain concentration by notches and cracks. J. Appl. Mech. 35 (1968), 379-386
- (6) Anderson, G.P., Ruggles, V.L., Stibor, G.S.: Use of finite element computer programs in fracture mechanics. Int. J. Fracture Mech. 7 (1971), 63-76
- (7) Parks, D.M.: A stiffness derivative finite element technique for determination of crack tip stress intensity factors. Int. J. Fracture 10 (1974), 487-502
- (8) Hellen, T.K.: On the method of virtual crack extensions. Int. J. num. Meth. Engng. 9 (1975), 187-207
- (9) Rybicki, E.F., Kanninen, M.F.: A finite element calculation of stress intensity factors by a modified crack closure integral. Engng. Fracture Mech. 9 (1977), 931-938

- (10) de Lorenzi, H.G.: On the energy release rate and the J-Integral for 3-D crack configurations. *Int. J. Fracture* 19, (1982), 183-193
- (11) Bakker, A.: The Three-Dimensional J-Integral. Dissertation, Technische Hochschule Delft, 1984
- (12) Buchholz, F.-G, Meiners, B.: Lokale und globale Energiemethoden zur Berechnung bruchmechanischer Kennwerte mit ASKA. In: International FEM-Congress, Proc. of the XIVth Int. Congr., Baden-Baden, November 1985. Edt. by: IKOSS GmbH, Stuttgart, 1985, 331-364
- (13) Buchholz, F.-G. and Meiners, B.: On the Accuracy of the Modified Crack Closure Integral Method in Combination with Higher Order Finite Elements. In: Accuracy Estimates and Adaptive Refinements in Finite Elements Computations (ARFEC), Vol. 1, Proc. of the Int. Conf., Lisbon, Portugal, June 1984. Edt. by: CREST, Technical University of Lisbon, Lisbon, Portugal, 1984, 131-140
- (14) Buchholz, F.-G.: Improved Formulae for the Finite Element Calculation of the Strain Energy Release Rate by the Modified Crack Closure Integral Method. In: Accuracy, Reliability and Training in FEM Technology, (Ed.: J. Robinson), Proc. of the 4th World Congr. and Exhib. on Finite Element Methods, Interlaken, Switzerland, September 1984. Robinson and Associates, Dorset, GB, 1984, 650-659
- (15) Buchholz, F.-G., Grebner, H., Strathmeier, U.: Numerical Investigations of Crack Closure Integral and J-Integral Calculations for a Thermally Stressed Specimen. In: Proc. of the Symp. of Energy Release Rates and Path Independent Integrals in Defect and Fracture Mechanics, Bad Honnef, Fed. Rep. of Germany, January 1985. *Int. J. of Solids and Structures* (special issue, to appear)
- (16) Buck, K.E.: Zur Berechnung der Verschiebungen und Spannungen in rotationssymmetrischen Körpern unter beliebiger Belastung. Dissertation, Universität Stuttgart (1970)
- (17) Tada, H., Paris, P., Irwin, G.: The Stress Analysis of Cracks Handbook. Del Research Corporation, St. Louis, Missouri (1973) 28.1 und 28.3

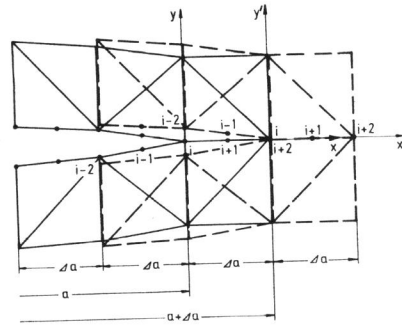
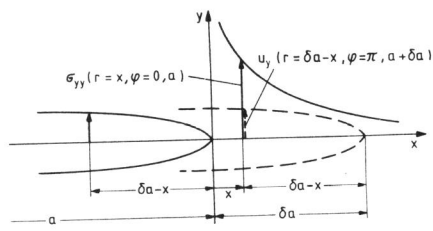


Figure 1 Analytical crack closure integral notations, $\lim \delta a \rightarrow 0$ Figure 2 Numerical crack closure integral notations, $\Delta a \gg 0$

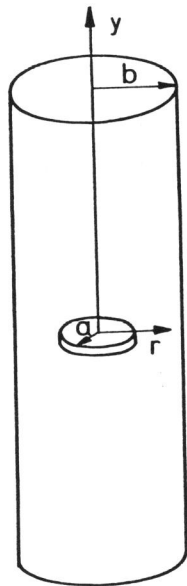


Figure 3 Penny-shaped crack in a cylinder

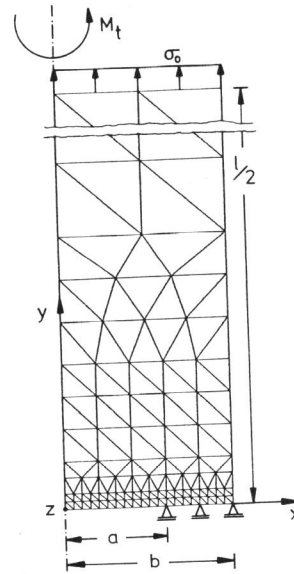


Figure 4 FE-discretisation; loading cases; boundary conditions

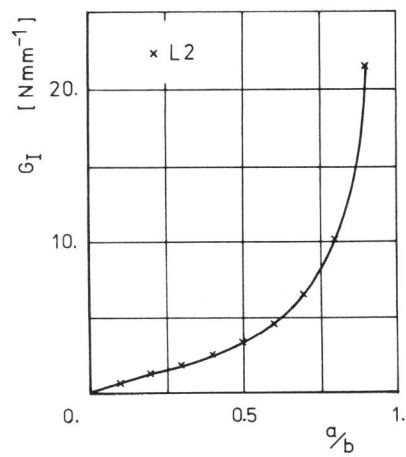


Figure 5 Energy release rate G_I (loading case 1)

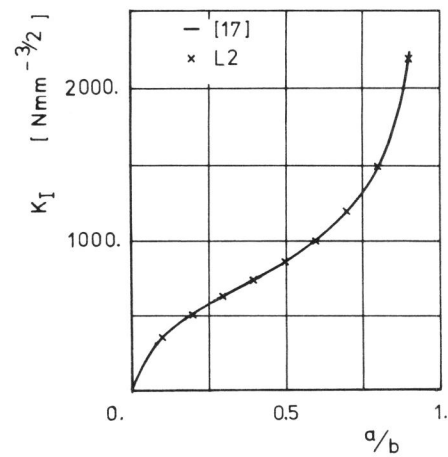


Figure 6 Stress intensity factor K_I (loading case 1)

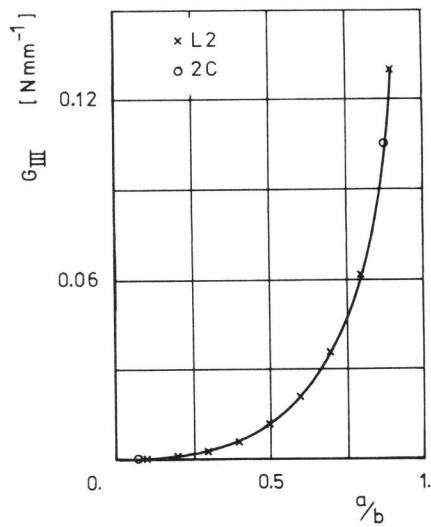


Figure 7 Energy release rate G_{III} (loading case 2)

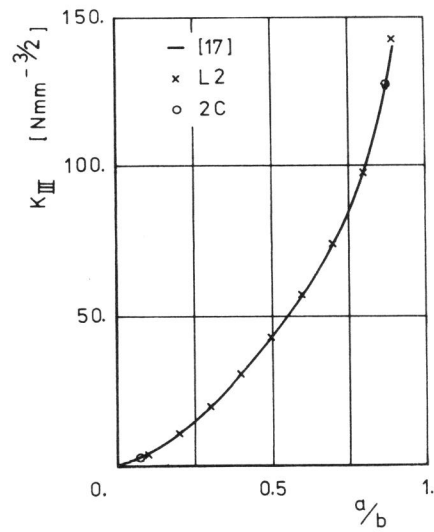


Figure 8 Stress intensity factor K_{III} (loading case 2)